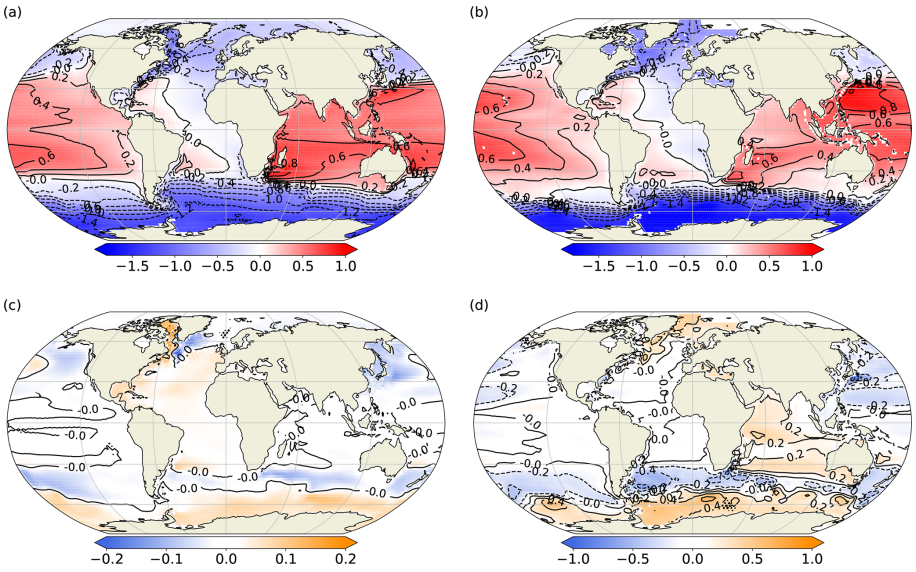

Figure 9. Time mean (years 2001–2025) of SSH (m) for **(a)** FORTE 2.0 L35 and **(b)** OCCA (2004–2006) climatology. Differences in SSH for **(c)** L20–L35 and **(d)** L35–OCCA.

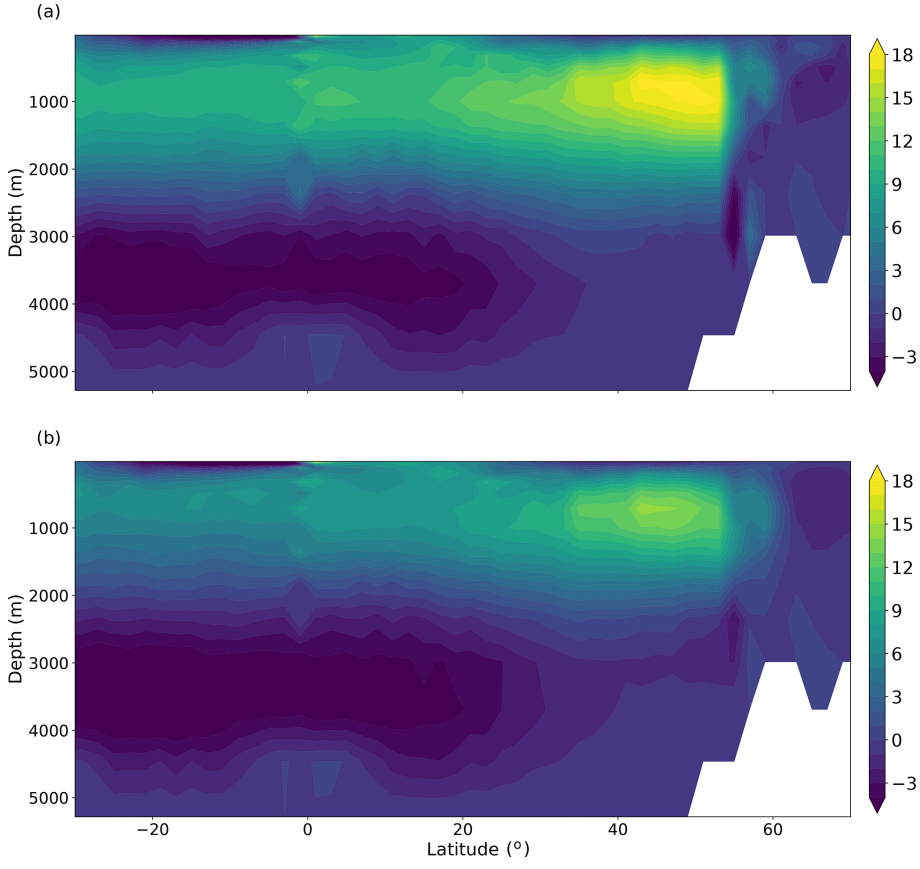

Figure 10. AMOC (Sv) as a function of latitude and depth, averaged over the years 1900–2025 of **(a)** the L35 integration and **(b)** the L20 integration.

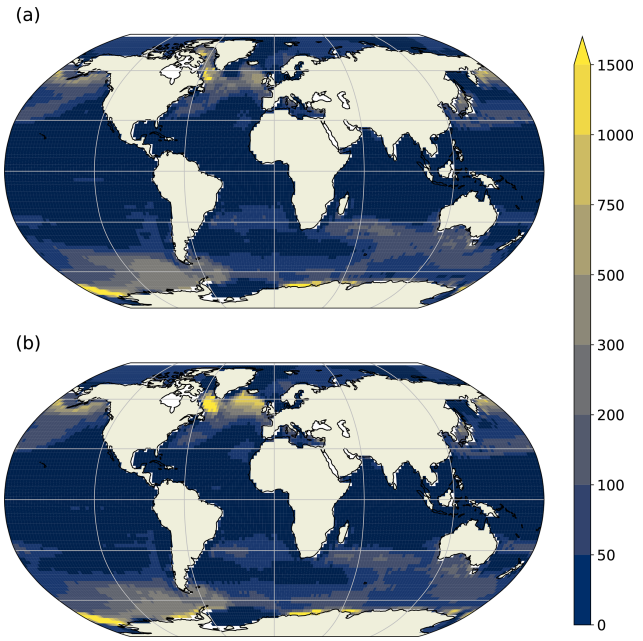

Figure 11. Winter mixed layer depths (m) averaged over the years 2000–2025 of **(a)** the L35 integration and **(b)** the L20 integration. The Northern (Southern) Hemisphere shows mixed layer depths for the month of March (September). The mixed layer depth is defined as the depth at which a density difference from the top layer of 0.03 kg m^{-3} occurs.

ern Pacific during JJA (Fig. 5d). A major difference with the observed distribution is the South Pacific ITCZ, which is narrow and predominantly zonal in the model solution, whereas observations show a broader northwest- to southeast-oriented region.

Contours of annual average mean sea level pressure, displayed in Fig. 6a, show the expected bands of high pressure over the subtropical oceans (e.g. the Azores and North Pacific highs) and over the polar regions and low pressure cells at midlatitudes (e.g. Icelandic and Aleutian lows) and over the equatorial regions. The seasonal range is largest over land (Fig. 6b), particularly highlighting the seasonal variability over Siberia. Differences in the annual mean sea level pressure anomalies and seasonal range (L20–L35) are predominantly poleward of 60° N and S (Fig. 6c and d). The seasonal range is smaller in L20 over the Labrador and GIN seas and over the high-latitude Southern Ocean. Contours of sea level pressure show the intensification of the surface winds over the midlatitudes in both the Southern Hemisphere and Northern Hemisphere during the winter season (Fig. 6e and f). We note that the Siberian High is not very intense for mean January conditions, and this appears to have the effect of allowing the Icelandic Low to expand and displace eastwards over Scandinavia, resulting in a displacement of the winter North Atlantic Oscillation (NAO) pattern compared with observations (see Sect. 5).

Time mean zonal wind for both summer and winter is shown in Fig. 7 as a function of latitude and pressure. The model exhibits Northern and Southern Hemisphere jet streams at around 40° S and 40° N at 200 hPa. The southern jet stream exhibits a lower seasonal range (28–36 m s^{-1}) than the northern jet stream (12–36 m s^{-1}). Surface westerlies and easterlies are of the order of ±0–4 m s^{-1} in the annual mean. The most notable differences between the L20 and L35 configurations occur during JJA, with weaker winds at 60° S. The midlatitude cores are also slightly stronger during JJA in L20. At 80° S, the zero contour extends down to the surface, indicating a change in the mean wind direction from weak westerlies to weak easterlies.

4.2 The ocean

Annual mean SST (Fig. 8a) shows maximum temperatures in the Indian and tropical Pacific and Atlantic oceans reach 26 °C. Compared with the EN3 climatology (Ingleby and Huddleston, 2007, Fig. 8c), there is a cool anomaly of around 1 °C throughout the tropics (Fig. 8e). Regions immediately west of the major land masses (coincident with regions of coastal upwelling) show warm SST errors of 2–3 °C magnitude, probably arising from a known issue in many coupled climate models related to the poor representation of marine stratocumulus clouds (Gordon et al., 2000). There is a substantial warm bias throughout the Southern Ocean and extending into the southern parts of the Pacific and Indian oceans, likely due to a combination of deficiencies in the physical representations of the ocean dynamics and cloud physics (Hyder et al., 2018). The Nordic Seas are several degrees cooler and up to 1.5 PSU fresher (Fig. 8f) than EN3, possibly due in part to the crude representation of sea ice, and in part due to the inadequate representation of ocean circulation in the Arctic and Nordic seas in a 2° resolution ocean model. There is a positive salinity bias of around 3 PSU further east in the Arctic, north of Siberia. Although large, the size of the salinity bias in the Arctic is not uncommon, even for models that do not require a polar island to prevent issues arising from the convergence of the grid at the North Pole (Megann et al., 2010). Annual mean SSS is well represented throughout the Southern Hemisphere ocean, where errors are mainly confined to within ±0.5 PSU (Fig. 8f). Positive biases of the order of 1–1.5 PSU occur in the Bay of Bengal and around the Maritime Continent and the northeast Pacific. The Labrador Sea and the region extending along the US coastline as far south as Cape Hatteras show positive salinity biases between 0.5 and 2 PSU, the latter coincident with a positive temperature bias that exceeds 5 °C in a small region that is indicative of the Gulf Stream separating too far north, bringing tropical waters too far north and west. It is worth noting, though, that the L20 simulation exhibits smaller biases in both SST and SSS in the Labrador and Irminger seas (Fig. 8g and h). There is also a slight improvement in the Southern Ocean warm bias in L20 com-

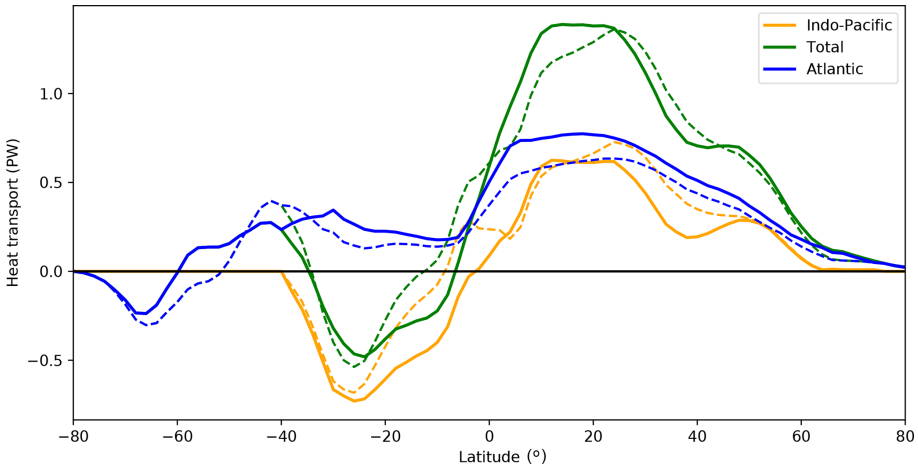

Figure 12. Meridional heat transport (PW) as a function of latitude for the global ocean, Atlantic and Indo-Pacific, averaged over the control integration. A five-grid-point smoother has been applied. Solid (dashed) lines show the meridional heat transport for the L35 (L20) simulation.

pared with L35. Some of the model biases will arise from the relatively coarse horizontal and vertical resolution and missing physical processes. However, as indicated by the differences between the L20 and L35 simulations, it is likely that a substantial reduction of biases would be achieved with the application of a rigorous calibration methodology such as history matching (Williamson et al., 2015).

Sea surface height (SSH) provides insight into the wind-driven ocean circulation. The SSH from L35 and the Ocean Comprehensible Atlas (OCCA; Forget, 2010) climatology are shown in Fig. 9a and b, respectively. Gyre circulation in all the major ocean basins is highlighted by the contours, along with regions of intensified flow, such as the Gulf Stream, the Kuroshio, and along the northern boundary of the ACC. However, the coarse resolution of the ocean model results in flows that are too broad and diffuse, weakening the SSH gradient across these intensified flows. The North Atlantic subpolar gyre appears constrained to the west of the basin. Slumping of the SSH gradient across the ACC is evident in the anomaly of L35 with respect to OCCA (Fig. 9d) and corresponds to the weak ACC transport shown earlier (Fig. 3). The slope in SSH is also weaker in the North Atlantic and extending into the Nordic Seas. Comparison with L20 (Fig. 9c) shows a slight steepening of the gradient across the ACC in L20, a small reduction in the bias compared with the OCCA climatology.

A latitude depth plot of the AMOC shows a maximum around 50° N and at 1000 m depth (Fig. 10). Closely packed streamlines at the high northern latitudes indicate that much of the deep convection occurs abruptly in a narrow latitude band and southward North Atlantic Deep Water transport reaches around 2.5 km depth. The abrupt sinking at the high northern latitudes is characteristic of coarse-resolution ocean models where flow into the Nordic Seas is poorly represented. Winter mixed layer depths in the southern Labrador Sea reach 2500 m in a few grid cells, whilst winter mixed layer depths south of the Denmark Strait, Iceland and the Faroe Bank Channel can reach 1000 m (Fig. 11). Wintertime convection is too shallow in the Nordic Seas, with mixed layer depths reaching 125–150 m in the central and eastern Nordic Seas. The AMOC transport through 30° S is 10 Sv in L35 and 6 Sv in L20, and is stronger ($\sim$ 14 Sv (L35), $\sim$ 10 Sv (L20)) at 30° N. There is a strong AABW cell ($\sim$ 6 Sv) centred at 3500 m depth, which weakens to about 2 Sv at 30° N. As mentioned earlier, the AABW cell in L20 is slightly stronger, and in Fig. 10 it is shown to extend further north. There is evidence of two-grid-point noise at the Equator, which has been identified previously in Bryan–Cox models (Weaver and Sarachik, 1990). The structure of the AMOC is similar in both the L35 and L20 simulations, with the L20 configuration consistently around 30 % weaker.

Ocean meridional heat transport (OHT) in FORTE 2.0 is around 60 % of that expected based on observational estimates but consistent with the weaker-than-observed volume transport (Fig. 12). Atlantic OHT at 26° N is 0.74 PW in L35 and 0.63 PW in L20, whilst observationally derived estimates suggest the current value is closer to 1.3 PW (Johns et al., 2011). Globally, the OHT reaches 1.4 PW, instead of the 2.1 ± 0.3 PW computed by Trenberth and Caron (2001). Over the Southern Ocean (35–65° S), OHT is northward, a characteristic seen previously in MOM-based ocean models (de Freitas Assad et al., 2009). This may be related to the strong warm SST bias present over the region at 40–60° S (Fig. 8) and its consequent effect on surface heat fluxes.

5 Modes of variability

A primary aim for any climate model is to adequately reproduce observed modes of climate variability sufficiently well that the model can be used to study the observed phenomena

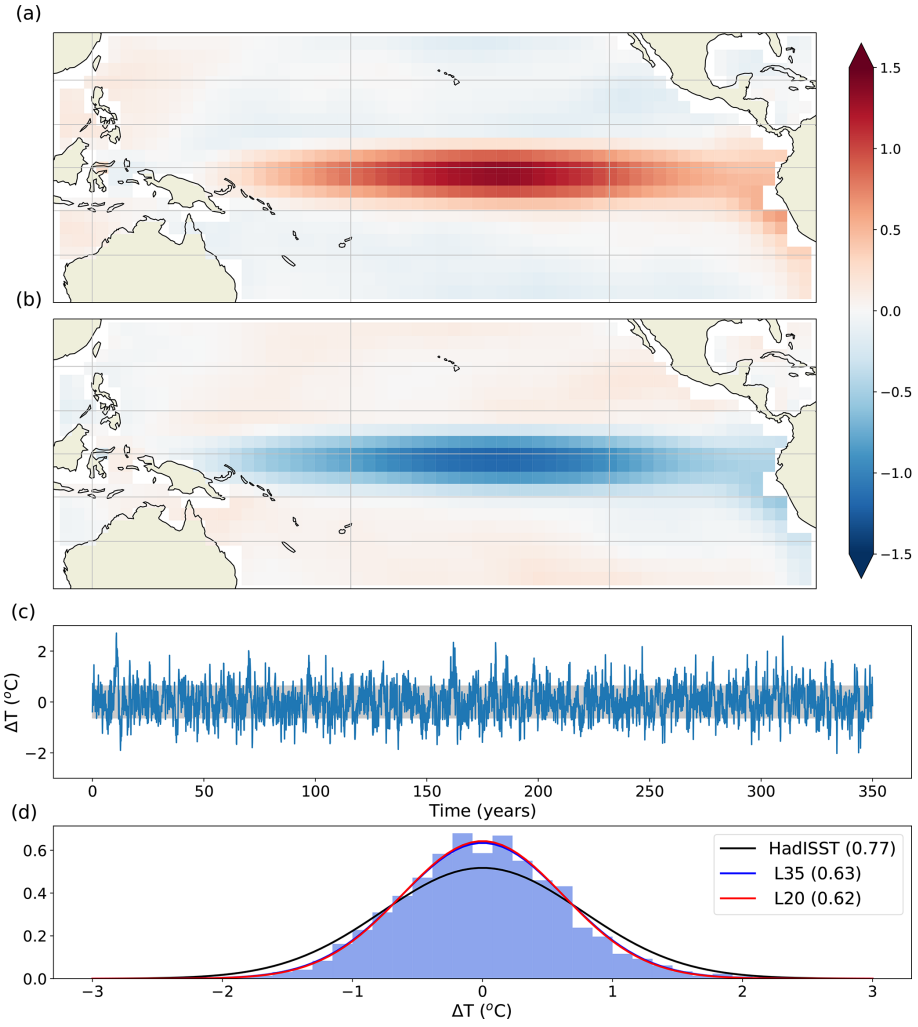

Figure 13. Composite anomaly of **(a)** El Niño events and **(b)** La Niña events from the L35 simulation. El Niño–Southern Oscillation (ENSO) events are defined as those which exceed ±1 standard deviation anomaly within the Niño 3.4 region. **(c)** SST anomaly time series and **(d)** histogram of SST anomaly distribution relative to the mean for the years 1601–1950 from the L35 simulation. The Gaussian curves in panel **(d)** are fits to the distribution of Niño 3.4 SST anomalies for HadISST (black, Trenberth (2020)), L35 (blue) and L20 (red). The blue and red lines are very close and the red line mostly overlies the blue line. Standard deviations are given in brackets.

in a variety of contexts. In this section, we present analysis of some of the most important modes using monthly mean ocean output for the years 1600–1950 of the control simulation and daily surface pressure output during the years 1600–1699 of the control integration.

Composites of the SST anomaly during El Niño and La Niña years show the spatial pattern of the anomalies throughout the tropics (Fig. 13a, b). Both phases of the El Niño–Southern Oscillation (ENSO) are weaker than observed, in particular near the eastern boundary. The composite temperature anomaly reaches a maximum of 1 °C for the region of 5° S–5° N, 160–100° W, whilst the characteristic region of observed strong SST anomalies near to the coast of Central and South America only reaches 0.7 °C and is not strongly connected to the warm anomaly in the central Pacific. This is probably related to the fact that the South Pacific Convergence Zone is too zonal and extends all the way across the Pacific, which is a common feature in coupled climate models (Niznik et al., 2015). The time series of temperature anomalies in the Niño 3.4 region shows a number of strong temperature anomaly events, although the magnitude is in general too small (Fig. 13c, d). We plot the distribution of SST anomalies for the Niño 3.4 region for both model configurations and for HadISST data for the period 1870–2019 (Rayner et al., 2003; Trenberth, 2020). The distribution of the histogram is too narrow compared with observations (Fig. 13d), and there is very little difference between the distributions for the L20 and L35 simulations. In both model configurations, the extreme values extend to around ±2 °C

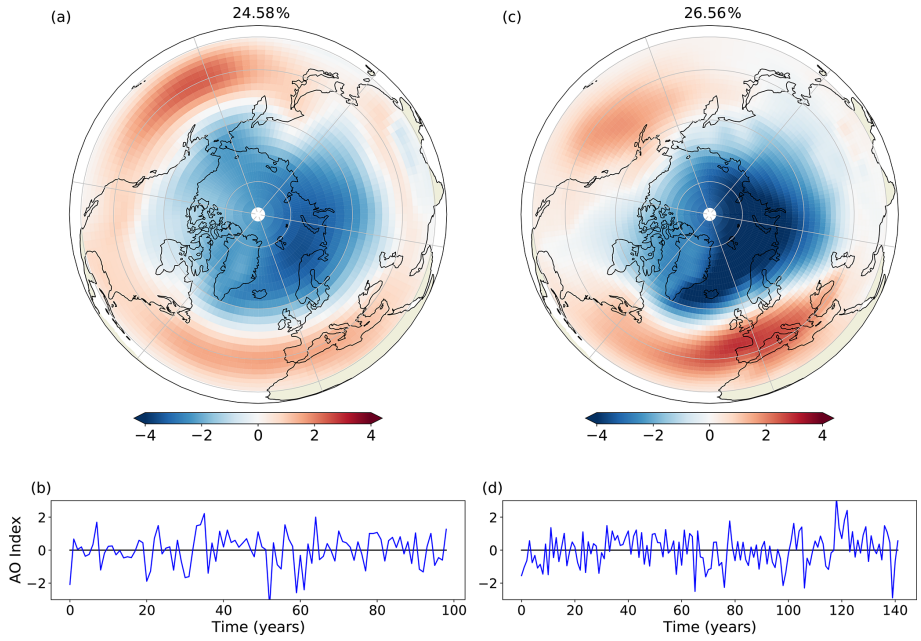

Figure 14. The AO as represented by the first EOF and PC computed using deseasoned and latitude-weighted sea level pressure for FORTE 2.0 **(a, b)** and 20CR **(c, d)**.

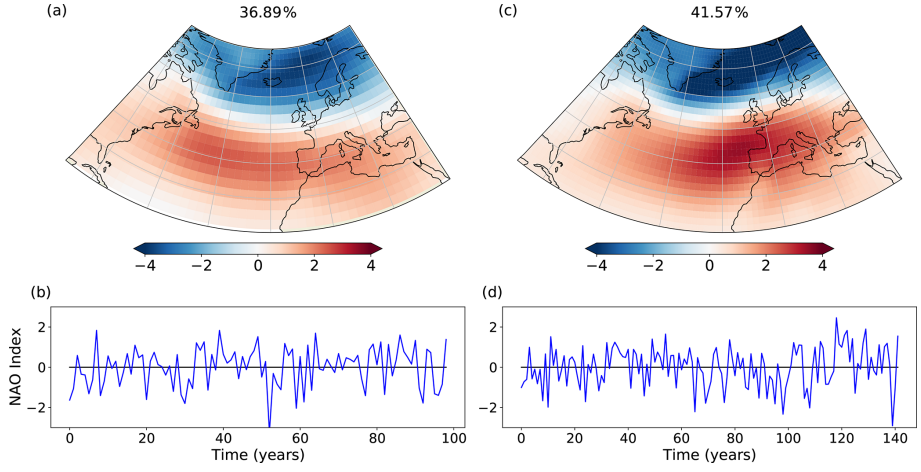

Figure 15. The NAO as represented by the first EOF and PC computed using deseasoned and latitude-weighted sea level pressure for FORTE 2.0 **(a, b)** and 20CR **(c, d)**.

(Fig. 13d), whilst observations suggest the extremes should be closer to ±2.5 °C.

We also examine the main extratropical modes of variability predicted by FORTE 2.0 in the Northern Hemisphere. We compare 20–90° N in an area-weighted empirical orthogonal function (EOF) analysis of the deseasoned and latitude-weighted sea level pressure fields from FORTE 2.0 and 20CR. FORTE 2.0 produces an annular mode structure as the main mode of variability, corresponding to the Arctic Oscillation (AO) in observed data. In agreement with observations (e.g. Thompson and Wallace, 2000; Ambaum et al., 2001), the model reproduces the two midlatitude centres of action over the North Pacific and North Atlantic, with the Pacific centre stronger and the Atlantic centre slightly weaker than those seen in the 20CR and the locations of their maxima displaced westward towards the western half of each ocean basin (Fig. 14). The strength of the Arctic pole in FORTE 2.0 is also weaker than in observations. The NAO is closely related to the AO and is one of the principal modes of atmospheric variability in the North Atlantic sector (Hurrell, 1995). We compute area-weighted EOFs for the NAO over the region of 20–80° N, 90° W–40° E. The first EOF and its accompanying principal component are presented in Fig. 15. In the North Atlantic, there is a good approximation to the

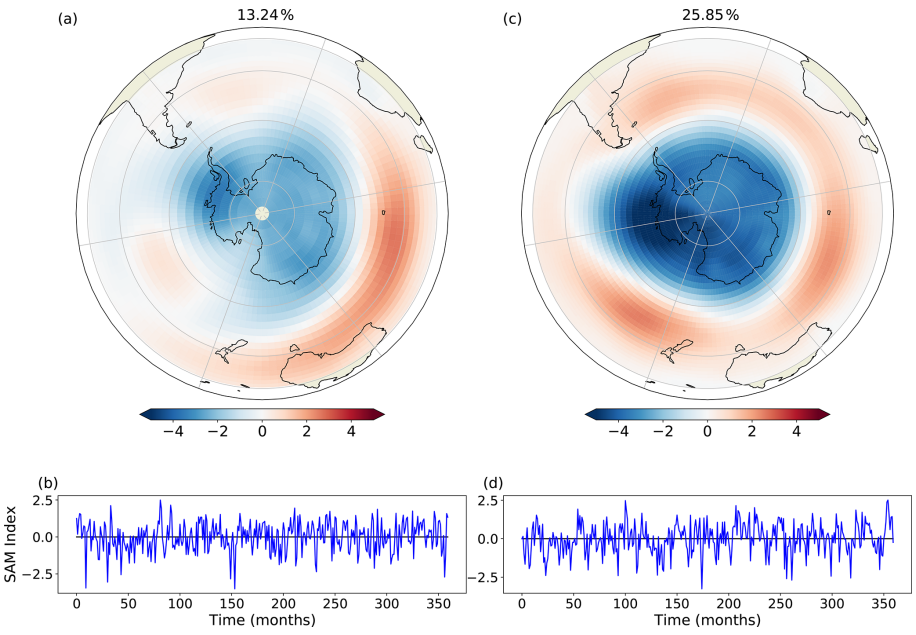

Figure 16. The SAM as represented by the first EOF and PC computed using deseasoned and latitude-weighted sea level pressure for FORTE 2.0 **(a, b)** and 20CR **(c, d)**.

NAO pattern, but in FORTE 2.0 the centre of the southern lobe is displaced westward and the northern lobe extends further south over mainland Europe compared with the observed pattern. Again, the principal component suggests more high-frequency variability in observations than in FORTE 2.0.

Similar to the Northern Hemisphere, the Southern Annular Mode (SAM) or Antarctic Oscillation represents the principal mode of climate variability in the Southern Hemisphere. Here, we compute area-weighted EOFs over the region of 20–90° S. FORTE 2.0 does not perform as well in the Southern Hemisphere (Fig. 16), with the annular structure significantly weaker over the Pacific and Atlantic sectors. The variance explained by the first EOF is also greatly reduced in FORTE 2.0, approximately half that seen in the 20CR, and this is likely to be linked with the anomalously warm Southern Ocean SST.

6 Summary

We present an assessment of two 2000-year simulations of the FORTE 2.0 coupled climate model: one using the 35σ layer atmosphere including a stratosphere (L35) and one using the 20σ layer atmosphere without a stratosphere (L20). The model integrates from rest and is sufficiently fast to enable studies of multi-centennial climate variability. The model is economic to run and can be adapted and configured to study a wide range of climate questions.

The simulations presented here are not optimally tuned for any specific purpose, but our assessment indicates that FORTE 2.0 is able to simulate a satisfactory climate state and climate variability. Biases that develop in the mean state are comparable to those found in other coupled climate models (Flato et al., 2013) and particularly those of similar complexity and resolution. A small imbalance in the freshwater budget (see Fig. 2) would need to be addressed for studies extending over timescales much longer than several millennia. Modes of climate variability in the Northern Hemisphere are represented well, though there are shortcomings in the Southern Hemisphere variability that are likely related to a strong SST bias over the Southern Ocean. Identifying the cause(s) of such biases is often a complex process in itself (Hyder et al., 2018) and beyond the scope of this current work. A further step would be to rigorously calibrate the model to improve the simulated climate and to better understand the limitations and behaviour of the modelled climate system.

Code availability. The code, compilation instructions and example run scripts, together with all necessary ancillary files, are accessible at https://doi.org/10.5281/zenodo.4108373 (Blaker et al., 2020). The configuration committed to the Zenodo archive (v2.0.1) is the one used to produce both of the simulations presented in this paper. Readers are advised that there is an error in the IGCM4 compile scripts archived as version 2.0 as linked in the discussion version of this paper. New users are advised to check the latest version of the code, which can be found at https://doi.org/10.5281/zenodo.3632568 (Blaker et al., 2020). Processing of the IGCM4 output requires the BGFLUX programme, a copy of which is accessible from the FORTE 2.0 GitHub repository linked to the Zenodo archive. A comprehensive user guide/manual for FORTE 2.0 does not currently exist. A folder titled "Documentation" has been added to the FORTE 2.0 GitHub repository, and

this contains relevant references and copies of technical documents from the original FORTE and component models.

Data availability. The code and data required to reproduce the figures presented in this paper are provided in the Supplement.

Supplement. The supplement related to this article is available online at: https://doi.org/10.5194/gmd-14-275-2021-supplement.

Author contributions. ATB, MJ and BS developed the coupled model configuration from versions used in earlier studies. The original coupling of FORTE was performed by BS and RSS. All authors were involved in finalising the configuration presented here. MJ undertook all model simulations. ATB wrote the paper, analysed the output and prepared all tables and figures. All authors edited the paper text.

Competing interests. The authors declare that they have no conflict of interest.

Acknowledgements. We acknowledge the support of resources provided by the high-performance computing cluster supported by the Research and Specialist Computing Support service at the University of East Anglia. We also acknowledge the support and contributions from colleagues on earlier versions of the code and simulations, most notably Matthew Brand, Craig Wallace and Marc Stringer. We gratefully acknowledge the developers of the software packages PVM and OASIS2.3, both of which are instrumental in the coupling for FORTE 2.0. We thank the editor and reviewers for their contributions. We also acknowledge William Dow, who retrieved and installed FORTE 2.0 from the repository and provided useful feedback to improve the installation instructions.

Financial support. This research has been supported by the Natural Environment Research Council. Adam T. Blaker, Joël J.-M. Hirschi and Bablu Sinha received support from ACSIS (NE/N018044/1); Bablu Sinha was also supported by SMURPHS (NE/N005686/2). Manoj Joshi was partially funded by SMURPHS (NE/N006348/1).

Review statement. This paper was edited by Julia Hargreaves and reviewed by two anonymous referees.

References

Ambaum, M. H. P., Hoskins, B. J., and Stephenson, D. B.: Arctic Oscillation or North Atlantic Oscillation?, J. Climate, 14, 3495–3507, 2001.

Arakawa, A.: Computational design for long-term numerical integrations of the equations of atmospheric motion, J. Comput. Phys., 1, 119–143, 1966.

Atkinson, C. P., Wells, N. C., Blaker, A. T., Sinha, B., and Ivchenko, V. O.: Rapid ocean wave teleconnections linking Antarctic salinity anomalies to the equatorial ocean-atmosphere system, Geophys. Res. Lett., 36, L08603, https://doi.org/10.1029/2008GL036976, 2009.

Beadling, R. L., Russell, J. L., Stouffer, R. J., Mazloff, M., Talley, L. D., Goodman, P. J., Sallée, J. B., Hewitt, H. T., Hyder, P., and Pandde, A.: Representation of Southern Ocean Properties across Coupled Model Intercomparison Project Generations: CMIP3 to CMIP6, J. Climate, 33, 6555–6581, https://doi.org/10.1175/JCLI-D-19-0970.1, 2020.

Betts, A. K. and Miller, M. J.: The Betts-Miller scheme, in: The Representation of Cumulus Convection in Numerical Models of the Atmosphere, Chapter 9, edited by: Emanuel, K. A. and Raymond, D. J., Amer. Meteor. Soc., Meteor. Mon., 24, 107–121, 1993.

Blaker, A., Joshi, M., Sinha, B., Stevens, D., Smith, R., and Hirschi, J.: NOC-MSM/FORTE 2.0: FORTE 2.0: a fast, parallel and flexible coupled climate model (Version v2.0.1), Zenodo, https://doi.org/10.5281/zenodo.4108373, 2020.

Blaker, A. T., Sinha, B., Ivchenko, V. O., Wells, N. C., and Zalesny, V. B.: Identifying the roles of the ocean and atmosphere in creating a rapid equatorial response to a Southern Ocean anomaly, Geophys. Res. Lett., 33, L06720, https://doi.org/10.1029/2005GL025474, 2006.

Blaker, A., Joshi, M., Sinha, B., Stevens, D., Smith, R., and Hirschi, J.: NOC-MSM/FORTE2.0: FORTE 2.0: a fast, parallel and flexible coupled climate model, Zenodo, https://doi.org/10.5281/zenodo.3632568, 2020.

Buchan, J., Hirschi, J. J.-M., Blaker, A. T., and Sinha, B.: North Atlantic SST anomalies and the cold North European weather events of winter 2009/10 and December 2010, Mon. Weather Rev., 142, 922–932, https://doi.org/10.1175/MWR-D-13-00104.1, 2014.

Compo, G. P., S.Whitaker, J., Sardeshmukh, P. D., Matsui, N., Allan, R. J., Yin, X., B. E. Gleason, J., Vose, R. S., Rutledge, G., Bessemoulin, P., Brönnimann, S., Brunet, M., Crouthamel, R. I., Grant, A. N., Groisman, P. Y., Jones, P. D., Kruk, M. C., Kruger, A. C., Marshall, G. J., Maugeri, M., Mok, H. Y., Nordli, Ø., Ross, T. F., Trigo, R. M., Wang, X. L., Woodruff, S. D., and Worley, S. J.: The Twentieth Century Reanalysis Project, Q. J. Roy. Meteor. Soc., 137, 1–28, 2011.

Cunningham, S. A., Alderson, S., King, B., and Brandon, M.: Transport and variability of the Antarctic Circumpolar Current in Drake Passage, J. Geophys. Res., 108, 8084, https://doi.org/10.1029/2001JC001147, 2003.

Danabasoglu, G. and McWilliams, J. C.: Sensitivity of the global ocean circulation to parameterizations of mesoscale tracer transports, J. Climate, 8, 2967–2987, 1995.

de Freitas Assad, L. P., Torres, A. R., Arruda, W. Z., da Silveira Mascarenhas, A., and Landau, L.: Volume and heat transports in the world oceans from an ocean general circulation model, Brazilian J. Geophys., 27, 181–194, https://doi.org/10.1590/S0102-261X2009000200003, 2009.

Donohue, K. A., Tracey, K. L., Watts, D. R., Chidichimo, M. P., and Chereskin, T. K.: Mean Antarctic Circumpolar Current transport measured in Drake Passage, Geophys. Res. Lett., 43, 11760–11767, https://doi.org/10.1002/2016GL070319, 2016.

ETOPO5: Global $5' \times 5'$ depth and elevation. Technical report, National Geophysical Data Centre, NOAA, US Department of Commerce, Boulder, USA, 1988.

Eyring, V., Bony, S., Meehl, G. A., Senior, C. A., Stevens, B., Stouffer, R. J., and Taylor, K. E.: Overview of the Coupled Model Intercomparison Project Phase 6 (CMIP6) experimental design and organization, Geosci. Model Dev., 9, 1937–1958, https://doi.org/10.5194/gmd-9-1937-2016, 2016.

Flato, G., Marotzke, J., Abiodun, B., Braconnot, P., Chou, S. C., Collins, W., Cox, P., Driouech, F., Emori, S., Eyring, V., Forest, C., Gleckler, P., Guilyardi, E., Jakob, C., Kattsov, V., Reason, C., and Rummukainen, M.: Evaluation of climate models, pp. 741–882, edited by: Stocker, T. F., Qin, D., Plattner, G.-K., Tignor, M., Allen, S. K., Doschung, J., Nauels, A., Xia, Y., Bex, V., and Midgley, P. M., Cambridge University Press, Cambridge, UK, https://doi.org/10.1017/CBO9781107415324.020, 2013.

Forget, G.: Mapping Ocean Observations in a Dynamical Framework: A 2004–06 Ocean Atlas, J. Phys. Oceanogr., 40, 1201–1221, https://doi.org/10.1175/2009JPO4043.1, 2010.

Forster, P. M., Blackburn, M., and Glover, R.: An examination of climate sensitivity for idealised climate change experiments in an intermediate general circulation model, Clim. Dynam., 16, 833–849, 2000.

Gargett, A. E.: Vertical eddy diffusivity in the ocean interior, J. Marine Res., 42, 359–393, https://doi.org/10.1357/002224084788502756, 1984.

Geist, A., Beguelin, A., Dongarra, J., Jiang, W., Manchek, R., and Sunderam, V.: PVM: parallel virtual machine, MIT Press, Cambridge, Massachusetts, 1994.

Gent, P. R. and McWilliams, J. C.: Isopycnal mixing in ocean circulation models, J. Phys. Oceanogr., 20, 150–155, 1990.

Gordon, C., Cooper, C., Senior, C., Banks, H., Gregory, J., Johns, T., Mitchell, J., and Wood, R.: The simulation of SST, sea ice extents and ocean heat transports in a version of the Hadley Centre coupled model without flux adjustments, Clim. Dynam., 16, 147–168, 2000.

Griffies, S. M.: The Gent-McWilliams skew flux, J. Phys. Oceanogr., 28, 831–841, 1998.

Griffies, S. M., Gnanadesikan, A., Pacanowski, R. C., Larichev, V., Dukowicz, J., and Smith, R.: Isoneutral diffusion in a z-coordinate ocean model, J. Phys. Oceanogr., 28, 805–830, 1998.

Grist, J. P., Josey, S. A., Sinha, B., and Blaker, A. T.: Response of the Denmark Strait overflow to Nordic Seas heat loss, J. Geophys. Res., 113, C09019, https://doi.org/10.1029/2007JC004625, 2008.

Haarsma, R. J., Selten, F. M., Opsteegh, J. D., Lenderink, G., and Liu, Q.: A coupled Atmosphere Ocean Sea-ice model for climate predictability studies, Technical Report, KNMI, the Netherlands, 1996.

Haarsma, R. J., Roberts, M. J., Vidale, P. L., Senior, C. A., Bellucci, A., Bao, Q., Chang, P., Corti, S., Fučkar, N. S., Guemas, V., von Hardenberg, J., Hazeleger, W., Kodama, C., Koenigk, T., Leung, L. R., Lu, J., Luo, J.-J., Mao, J., Mizielinski, M. S., Mizuta, R., Nobre, P., Satoh, M., Scoccimarro, E., Semmler, T., Small, J., and von Storch, J.-S.: High Resolution Model Intercomparison Project (HighResMIP v1.0) for CMIP6, Geosci. Model Dev., 9, 4185–4208, https://doi.org/10.5194/gmd-9-4185-2016, 2016.

Heuzé, C., Heywood, K., Stevens, D., and Ridley, J.: Changes in Global Ocean Bottom Properties and Volume Transports in CMIP5 Models under Climate Change Scenarios, J. Climate, 28, 2917–2944, https://doi.org/10.1175/JCLI-D-14-00381.1, 2015.

Hunt, F. K., Hirschi, J. J.-M., Sinha, B., Oliver, K., and Wells, N.: Combining point correlation maps with self-organising maps to compare observed and simulated atmospheric teleconnection patterns, Tellus A, 65, 20822, https://doi.org/10.3402/tellusa.v65i0.20822, 2013.

Hurrell, J. W.: Decadal trends in the North Atlantic Oscillation regional temperatures and precipitation, Science, 269, 676–679, 1995.

Hyder, P., Edwards, J. M., Allan, R. P., Hewitt, H. T., Bracegirdle, T. J., Gregory, J. M., Wood, R. A., Meijers, A. J. S., Mulcahy, J., Field, P., Furtado, K., Bodas-Salcedo, A., Williams, K. D., Copsey, D., Josey, S. A., Liu, C., Roberts, C. D., Sanchez, C., Ridley, J., Thorpe, L., Hardiman, S. C., Mayer, M., Berry, D. I., and Belcher, S. E.: Critical Southern Ocean climate model biases traced to atmospheric model cloud errors, Nat. Commun., 9, 3625, https://doi.org/10.1038/s41467-018-05634-2, 2018.

Ingleby, B. and Huddleston, M.: Quality control of ocean temperature and salinity profiles – historical and real-time data, J. Marine Syst., 65, 158–175, https://doi.org/10.1016/j.jmarsys.2005.11.019, 2007.

Johns, T. C., Durman, C. F., Banks, H. T., Roberts, M. J., McLaren, A. J., Ridley, J. K., Senior, C. A., Williams, K. D., Jones, A., Rickard, G. J., Cusack, S., Ingram, W. J., Crucifix, M., Sexton, D. M. H., Joshi, M. M., Dong, B. W., Spencer, H., Hill, R. S. R., Gregory, J. M., Keen, A. B., Pardaens, A. K., Lowe, J. A., Bodas-Salcedo, A., and Stark, S.: The New Hadley Centre Climate Model (HadGEM1): Evaluation of Coupled Simulations, J. Climate, 19, 1327–1353, 2006.

Johns, W. E., Baringer, M. O., Beal, L. M., Cunningham, S. A., Kanzow, T., Bryden, H. L., Hirschi, J. J.-M., Marotzke, J., Meinen, C., Shaw, B., and Curry, R.: Continuous, array-based estimates of Atlantic Ocean heat transport at 26.5N, J. Climate, 24, 2429–2449, https://doi.org/10.1175/2010JCLI3997.1, 2011.

Joshi, M., Stringer, M., van der Wiel, K., O'Callaghan, A., and Fueglistaler, S.: IGCM4: a fast, parallel and flexible intermediate climate model, Geosci. Model Dev., 8, 1157–1167, https://doi.org/10.5194/gmd-8-1157-2015, 2015.

Killworth, P. D., Stainforth, D., Webb, D. J., and Paterson, S. M.: The development of a free-surface Bryan-Cox-Semtner ocean model, J. Phys. Oceanogr., 21, 1333–1348, 1991.

Kuhlbrodt, T., Smith, R., Wang, Z., and Gregory, J.: The influence of eddy parameterizations on the transport of the Antarctic Circumpolar Current in coupled climate models, Ocean Model., 52-53, 1–8, 2012.

Levitus, S. and Boyer, T. P.: World Ocean Atlas 1998, Volume 4, Temperature, NOAA Atlas, NESDIS 2, 99 pp., 1998.

Levitus, S., Burgett, R., and Boyer, T. P.: World Ocean Atlas 1998, Volume 3, Salinity, NOAA Atlas, NESDIS 3, 99 pp., 1998.

Marsh, R., Hazeleger, W., Yool, A., and Rohling, E. J.: Stability of the thermohaline circulation under millennial CO_2 forcing and two alternative controls on Atlantic salinity, Geophys. Res. Lett., 34, L03605, https://doi.org/10.1029/2006GL027815, 2007.

McCarthy, G., Frajka-Williams, E., Johns, W. E., Baringer, M. O., Meinen, C. S., Bryden, H. L., Rayner, D., Duchez, A., Roberts, C., and Cunningham, S. A.: Observed interannual variability of the Atlantic meridional overturning

circulation at 26.5° N, Geophys. Res. Lett., 39, L19609, https://doi.org/10.1029/2012GL052933, 2012.

Meehl, G. A., Covey, C., Delworth, T., Latif, M., McAvaney, B., Mitchell, J., Stouffer, R., and Taylor, K.: The WCRP CMIP3 Multimodel Dataset: A New Era in Climate Change Research, B. Am. Meteorol. Soc., 88, 1383–1394, 2007.

Megann, A. P., New, A. L., Blaker, A. T., and Sinha, B.: The CHIME coupled climate model, J. Climate, 23, 5126–5150, https://doi.org/10.1175/2010JCLI3394.1, 2010.

Montoya, M., Griesel, A., Levermann, A., Mignot, J., Hofmann, M., Ganopolski, A., and Rahmstorf, S.: The earth system model of intermediate complexity CLIMBER-3-alpha. Part I: description and performance for present-day conditions, Clim. Dynam., 25, 237–263, https://doi.org/10.1007/s00382-005-0044-1, 2005.

Niznik, M. J., Lintner, B., Matthews, A., and Widlansky, M.: The Role of Tropical–Extratropical Interaction and Synoptic Variability in Maintaining the South Pacific Convergence Zone in CMIP5 Models, J. Climate, 28, 3353–3374, https://doi.org/10.1175/JCLI-D-14-00527.1, 2015.

Pacanowski, R. C., Dixon, K., and Rosati, A.: The GFDL modular ocean model users guide: version 1.0, GFDL Group Technical Report No. 2, Tech. rep., NOAA/Geophysical Fluid Dynamics Laboratory, Princeton University, Princeton, NJ, variously paged, 1990.

Rayner, N. A., Parker, D. E., Horton, E. B., Folland, C. K., Alexander, L. V., Rowell, D. P., Kent, E. C., and Kaplan, A.: Global analyses of sea surface temperature, sea ice, and night marine air temperature since the late nineteenth century, J. Geophys. Res., 108, 4407, https://doi.org/10.1029/2002JD002670, 2003.

Roberts, M. J., Baker, A., Blockley, E. W., Calvert, D., Coward, A., Hewitt, H. T., Jackson, L. C., Kuhlbrodt, T., Mathiot, P., Roberts, C. D., Schiemann, R., Seddon, J., Vannière, B., and Vidale, P. L.: Description of the resolution hierarchy of the global coupled HadGEM3-GC3.1 model as used in CMIP6 HighResMIP experiments, Geosci. Model Dev., 12, 4999–5028, https://doi.org/10.5194/gmd-12-4999-2019, 2019.

Sellar, A. A., Jones, C. G., Mulcahy, J. P., Tang, Y., Yool, A., Wiltshire, A., O'Connor, F. M., Stringer, M., Hill, R., Palmieri, J., Woodward, S., de Mora, L., Kuhlbrodt, T., Rumbold, S. T., Kelley, D. I., Johnson, R. E. C. E., Walton, J., Abraham, N. L., Andrews, M. B., Andrews, T., Archibald, A. T., Berthou, S., Burke, E., Blockley, E., Dalvi, K. C. M., Edwards, J., Folberth, G. A., Gedney, N., Griffiths, P. T., Harper, A. B., Hendry, M. A., Hewitt, A. J., Johnson, B., Jones, A., Jones, C. D., Keeble, J., Liddicoat, S., Morgenstern, O., Parker, R. J., Predoi, V., Robertson, E., Siahaan, A., Smith, R. S., Swaminathan, R., Zeng, M. T. W. G., and Zerroukat, M.: UKESM1: Description and Evaluation of the U.K. Earth System Model, J. Adv. Model. Earth Syst., 11, 4513–4558, https://doi.org/10.1029/2019MS001739, 2019.

Shaffrey, L. C., Stevens, I., Norton, W. A., Roberts, M. J., Vidale, P. L., Harle, J. D., Jrrar, A., Stevens, D. P., Woodage, M. J., Demory, M. E., Donners, J., Clark, D. B., Clayton, A., Cole, J. W., Wilson, S. S., Connolley, W. M., Davies, T. M., Iwi, A. M., Johns, T. C., King, J. C., New, A. L., Slingo, J. M., Slingo, A., Steenman-Clark, L., and Martin, G. M.: UK-HiGEM: The New UK High Resolution Global Environment Model. Model description and basic evaluation, J. Climate, 22, 1861–1896, https://doi.org/10.1175/2008JCLI2508.1, 2009.

Sinha, B. and Smith, R.: Development of a fast Coupled General Circulation Model (FORTE) for climate studies, implemented using the OASIS coupler, Tech. rep., Southampton Oceanography Centre, Southampton, UK, Internal Document, No. 81, 67 pp., 2002.

Sinha, B., Blaker, A. T., Hirschi, J. J.-M., Bonham, S., Brand, M., Josey, S. A., Smith, R. S., and Marotzke, J.: Mountain ranges favour vigorous Atlantic meridional overturning, Geophys. Res. Lett., 39, L02705, https://doi.org/10.1029/2011GL050485, 2012.

Smith, R., Dubois, C., and Marotzke, J.: Ocean circulation and climate in an idealised Pangean OAGCM, Geophys. Res. Lett., 31, L18207, https://doi.org/10.1029/2004GL020643, 2004.

Smith, R., Dubois, C., and Marotzke, J.: Global Climate and Ocean Circulation on an Aquaplanet Ocean-Atmosphere General Circulation Model, J. Climate, 19, 4719–4737, 2006.

Smith, R. S., Gregory, J. M., and Osprey, A.: A description of the FAMOUS (version XDBUA) climate model and control run, Geosci. Model Dev., 1, 53–68, https://doi.org/10.5194/gmd-1-53-2008, 2008.

Taylor, K., Stouffer, R., and Meehl, G.: An Overview of CMIP5 and the experiment design, B. Am. Meteorol. Soc., 93, 485–498, https://doi.org/10.1175/BAMS-D-11-00094.1, 2012.

Terray, L., Valcke, S., and Piacentini, A.: The OASIS Coupler User Guide Version 2.3, Tech. Rep. TR/CMGC/99-37, Tech. rep., CERFACS, Toulouse, France, 1999.

Thompson, D. W. J. and Wallace, J. M.: Annular modes in the extratropical circulation. Part I: Month-to-month variability, J. Climate, 13, 1000–1016, 2000.

Trenberth, K. E.: The Climate Data Guide: Nino SST Indices (Nino 1+2, 3, 3.4, 4; ONI and TNI), available at: https://climatedataguide.ucar.edu/climate-data/nino-sst-indices-nino-12-3-34-4-oni-and-tni., last access: 10 July 2020.

Trenberth, K. E. and Caron, J. M.: Estimates of meridional atmosphere and ocean heat transports, J. Climate, 14, 3433–3443, 2001.

Weaver, A. J.: The UVic earth system climate model and the thermohaline circulation in past, present and future climates, IUGG 2003 General Assembly of the International Union of Geodesy and Geophysics No23, Sapporo, Geophysical monograph ISSN 0065-8448 CODEN GPMGAD, 150 (416 p.), 279–296, 2004.

Weaver, A. J. and Sarachik, E. S.: On the importance of vertical resolution in certain ocean general circulation models, J. Phys. Oceanogr., 20, 600–609, 1990.

Weaver, A. J., Eby, M., Augustus, F. F., and Wiebe, E. C.: Simulated influence of carbon dioxide, orbital forcing and ice sheets on the climate of the Last Glacial Maximum, Nature, 394, 847–853, 1998.

Webb, D. J.: An ocean model code for array processor computers, Comput. Geosci., 22, 569–578, 1996.

Webb, D. J., de Cuevas, B. A., and Richmond, C. S.: Improved Advection Schemes for Ocean Models, J. Atmos. Ocean. Tech., 15, 1171–1187, 1998.

Williamson, D., Blaker, A. T., Hampton, C., and Salter, J.: Identifying and removing structural biases in climate models with history matching, Clim. Dynam., 45, 1299–1324, https://doi.org/10.1007/s00382-014-2378-z, 2015.

Wilson, C., Sinha, B., and Williams, R. G.: The effect of ocean dynamics and orography on atmospheric storm tracks, J. Climate, 22, 3689–3702, https://doi.org/10.1175/2009JCLI2651.1, 2009.

Wu, J.: Wind-Stress Coefficients over Sea Surface near Neutral Conditions - A Revisit, J. Phys. Oceanogr., 10, 727–740, 1980.

Zhong, W. Y. and Haigh, J. D.: Improved broad-band emissivity parameterization for water vapor cooling calculations, J. Atmos. Sci., 52, 124–148, 1995.